Journal Name

ARTICLE TYPE

Cite this: DOI: 00.0000/xxxxxxxxxx

Buffer-specific effects arise from ionic dispersion forces

Drew F. Parsons,*[a,b‡] Cristina Carucci,[a] and Andrea Salis[a]

Received Date
Accepted Date

DOI: 00.0000/xxxxxxxxxx

Buffer solutions do not simply regulate pH, but also change the properties of protein molecules. The zeta potential of lysozyme varies significantly at the same buffer concentration, in the order Tris > phosphate > citrate, with citrate even inverting the zeta potential, usually positive at pH 7.15, to a negative value. This buffer-specific effect is a special case of the Hofmeister effect.
Here we present a theoretical model of these buffer-specific effects using a Poisson-Boltzmann description of the buffer solution, modified to include dispersion forces of all ions interacting with the lysozyme surface. Dispersion coefficients are determined from quantum chemical polarizabilites calculated for each ion for tris, phosphate, and citrate buffer solutions. The lysozyme surface charge is controlled by charge regulation of carboxylate and amine sites of the component amino acids. The theoretical model satisfactorily reproduces experimental zeta potentials, including change of sign with citrate, when hydration of small cosmotropic ions (Na^+, H^+, OH^-) is included.

1 Introduction

The influence of salt on interactions between particles in solution is a core question in engineering and biology. At the simplest level of modelling described by Poisson-Boltzmann or Debye-Hückel theory in the theory of Derjaguin-Landau, Verwey-Overbeek (DLVO), salt solutions affect surface forces solely through their ionic strength. But in real systems different salts affect surface forces in different ways. Such ion specificity was first described by Hofmeister in 1888, studying the solubility of egg white proteins in salt solutions.

Typically such Hofmeister effects are observed at ionic strengths exceeding 0.1M, approaching physiological salt concentrations[1,2]. But lower concentration Hofmeister effects have been found[3]. An intriguing special case is the observation of buffer-specific effects[4–8]. Routinely used in biochemical assays to control pH, buffer solutions are typically assumed to play no other role, although some adverse effects of specific buffers have been reported[9]. Buffers ions are either assumed to have negligible direct effect on substrate properties, apart from those such as surface charge that are determined by pH, or else the experimental protocol mandates a specific buffer solution with no freedom to employ an alternative buffer. Buffer specific effects can be surprisingly large, and may be even as extreme as inverting the sign of the zeta potential under the same low buffer strength of 10 mM[5].

In this work we briefly review buffer-specific effects observed experimentally, in particular zeta potentials measured for lysozyme. We then present theory to explain these buffer effects, using a Poisson-Boltzmann model modified to include dispersion interactions of buffer ions. Dispersion coefficients are evaluated from quantum chemical calculations of dynamic polarizabilities of each ion. We find that when the hydration state of small cosmotropic ions (Na^+, H^+, OH^-) is taken into account, the theory satisfactorily reproduces the observed trends in zeta potentials, including the change in sign observed with citrate buffer. The agreement between theory and experiment holds well both for pure buffer solutions (without added salt), and with added salt.

2 Buffer Specific Effects

Cugia et al. reported the electrophoretic mobility of lysozyme in various buffer solutions in 2013[5], presented later as zeta potentials[8]. 1 g/L of lysozyme was used with a buffer concentration of 10 mM set at pH 7.15. Anionic buffers were taken with Na^+ counterion, and the cationic buffer Tris was taken with Cl^- as counterion. Measurements were performed without and with added salt. Results for Tris, cacodylate, phosphate and citrate buffers without salt and with 100 mM added Na salts (NaCl, $NaNO_3$, NaSCN) are collated in Fig. 1.

Considering the case of pure buffer without added salt, a clear buffer-specific effect is observed even at the relatively low buffer concentration of 10 mM. In Tris buffer the zeta potential is measured at 20 mV, while in citrate buffer the the sign of the zeta potential is inverted at −7 mV. Phosphate buffer lies between, generating the buffer series Tris > cacodylate > phosphate > citrate.

[a] Department of Chemical and Geological Sciences, University of Cagliari, Cittadella Universitaria, S.S. 554 bivio Sestu, 09042 Monserrato (CA), Italy
[b] Murdoch University, Discipline of Physics, Chemistry and Mathematics, 90 South St, Murdoch, WA, AUS 6150
‡ E-mail: drew.parsons@unica.it

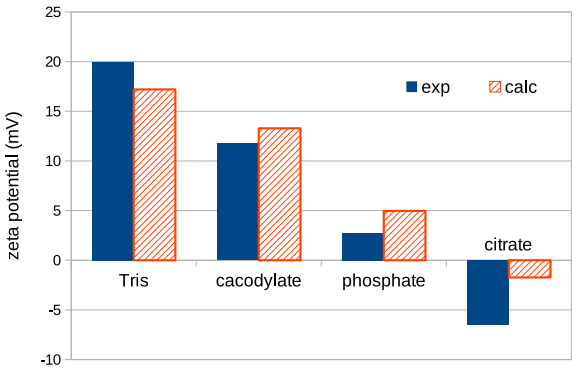

Fig. 1 Zeta potentials for 1g/L lysozyme in 10mM buffer at pH 7.15. Buffer solutions are Tris, cacodylate, phosphate, citrate. Experimental values shown in left bar (solid blue), theoretical values calculated in this work are shown in the right bars (striped red). Theoretical zeta potentials are evaluated at 3 water diameters from the protein surface.

The buffer-specific trends shown here in lysozyme zeta potentials have been found also in lysozyme adsorption on silica[8] (in the reverse order citrate > phosphate > Tris, indicating that a smaller positive lysozyme potential counterintuitively increases adsorption to the negatively charge silica surface). Buffer specificity is also observed in protein diffusivity[6,10], enzyme activity[11] and pH measurement[4].

3 Buffer Theory

We employ a Poisson-Boltzmann description of the electrolyte. Treating the lysozyme protein as a sphere with radius $R_p = 1.53$ nm[12], the electrostatic potential $\psi(x)$ outside the protein is determined from ion concentration profiles $c_i(x)$ by the Poisson equation in spherical coordinates with spherical symmetry,

$$-\varepsilon_0\varepsilon\,(x+R_p)^2\,\frac{d^2\psi}{dx^2} = -\sum_i z_i e c_i(x) \tag{1}$$

where $x = r - R_p$ is the radial distance from the protein surface, r is the radial distance from the centre of the protein. z_i is the valency of each ion, e is the elementary charge. i indexes each ion in the electrolyte, including buffer ions (or neutral species with $z_i = 0$), H^+ and OH^- and counterion Na^+ or Cl^- used to adjust buffer pH to 7.15 (adjusting pH with HCl or NaOH).

Ion (and neutral molecule) concentration profiles $c_i(x)$ are calculated using a Boltzmann relation describing equilibrium with bulk concentrations c_{i0},

$$c_i(x) = c_{i0}e^{-\left[z_i e\psi(x)+\mu_i^{\mathrm{NES}}(x)\right]/kT} \tag{2}$$

k is Boltzmann's constant and T is temperature, taken as 298.15 K (25°C). $z_i e\psi(z)$ describes the electrostatic potential energy of the ion. Eq. (1) and Eq. (2) together form the modified Poisson-Boltzmann model. $\mu_i^{\mathrm{NES}}(z)$ describes nonelectrostatic ion interactions, and distinguishes the model from the conventional Poisson-Boltzmann model which accounts only for the electostatic potential. For μ_i^{NES} we employ a model of ionic dispersion forces described in the next section.

Lastly, solution of the Poisson equation requires specification of boundary conditions. The slope of the potential at the protein surface is related to the surface charge σ,

$$\left.\frac{d\psi}{dx}\right|_{x=0} = -\frac{\sigma}{\varepsilon_0\varepsilon} \tag{3}$$

We employ a charge regulated model for surface charge controlled by pH, described below.

The domain of calculation extends away from the protein surface to a distance $z = L = 30\kappa^{-1}$, where κ^{-1} is the Debye length of the electrolyte. At a distance of $30\kappa^{-1}$ the solution is essentially bulk solution, represented by a zero-charge boundary condition, $\sigma_L = 0$,

3.1 Ionic Dispersion Forces

London dispersion forces describe the interactions of instantaneous dipoles formed by fluctuations in the electron cloud of a species due to their dynamic electron polarizability α_i. We invoke a theory of dispersion forces developed by Mahanty and Ninham[13,14], which includes finite-size effects by representing the ion as a polarizable Gaussian sphere with Gaussian radius a_i, embedded in a medium with dielectric function $\varepsilon(\omega)$. The dispersion interaction potential, adapted for spherical geometry[15], is taken as

$$\mu_i^{\mathrm{NES}}(z) = \frac{B_i g_i(x)}{x^3\left(1+(x/R_p)^3\right)} \tag{4}$$

$g_i(x)$ is a factor that describes finite size effects,

$$g_i(x) = 1 + \frac{2x}{\sqrt{\pi}a_i}\left[\frac{2x^2}{a_i^2} - 1\right]\exp\left(-\frac{x^2}{a_i^2}\right) - \left[1+\frac{4x^4}{a_i^4}\right]\mathrm{erfc}\left(\frac{x}{a_i}\right). \tag{5}$$

It was derived for the interaction of an ion with a planar interface and is not specifically adapted for a spherical geometry, but serves to render $\mu_i^{\mathrm{NES}}(x)$ finite at contact (at $x = 0$),

The dispersion coefficient B_i is evaluated using a variation of Lifshitz theory, summing the ion polarizability α_i and reflection coefficients Δ over imaginary frequencies corresponding to Matsubara energies $\hbar\omega_n = 2\pi nkT$ (the factor 2π is incorrectly missing in Ref. 16),

$$B_i = \frac{kT}{2}{\sum_n}' \frac{\alpha_i(i\omega_n)\Delta(i\omega_n)}{\varepsilon_w(i\omega_n)}, \tag{6}$$

$\Delta(i\omega)$ is the reflection coefficient for the virtual photons driving dispersion forces,

$$\Delta(i\omega) = \frac{\varepsilon_w(i\omega)-\varepsilon_p(i\omega)}{\varepsilon_p(i\omega)+\varepsilon_p(i\omega)}. \tag{7}$$

ε_w and ε_p are the dielectric functions for water and protein, respectively.

The polarizability α_i is the effective polarizability of the ion in the solvent medium (water). Here we determine α_i from the ion's intrinsic polarizability in vacuum, α_i^0 using a hard-sphere Clausius-Mossotti (or more precisely, Lorenz-Lorentz) relationship[17,18]

$$\alpha_i = 4\pi\varepsilon_0\varepsilon_w R_i^3\,\frac{\varepsilon_i-\varepsilon_w}{\varepsilon_i+2\varepsilon_w} \tag{8}$$

ε_i is an effective dielectric function for the ion taken as a hard

sphere, determined from the vacuum polarizability α_i^0,

$$\varepsilon_i = \frac{1+2\alpha_i^0/(4\pi\varepsilon_0 R_i^3)}{1-\alpha_i^0/(4\pi\varepsilon_0 R_i^3)} \tag{9}$$

R_i is the hard sphere radius of the ion, related to its Gaussian radius by equating the same ion volume[19], $R_i^3 = a_i^3 3\sqrt{\pi}/4$. At zero frequency, we also add the rotational polarizability $\alpha_{\rm rot} = \mu_0^2/3kT$ to the vacuum polarizability, where μ_0 is the permanent dipole of the ion.

Ion radii and dispersion B_i coefficients calculated by this method are listed in Table 1. We use a recent description of the dielectric function of water[16] that includes the far UV/soft X-ray spectrum, 20-100 eV. A detailed optical spectrum for lysozyme is not yet available, hence a simple generic protein model is employed[20].

We calculated intrinsic ion polarizabilities and dipole moments in vacuum using quantum chemical methods. Polarizabilities for simple ions have been reported previously[21]. Polarizabilites for buffer ions (and the neutral Tris base) were calculated in Turbomole[22] v7.2 by density functional theory (DFT) using a PBE0 functional[23] with augmented correlation-consistent basis sets[24,25], aug-cc-pVTZ. Dynamic polarizabilities at imaginary Matsubara frequencies were calculated up to $n = 2100$. In our calculations of B_i we used the exact values from quantum chemical calculations, but for convenience we also present in Table 2 a 5-oscillator model (4-oscillators for H_3O^+, Tris$-H^+$ and Tris), expected to provide around 0.001% error relative to quantum chemical values[21],

$$\alpha(i\omega) = \sum_i \frac{\alpha_i}{1+\omega^2/\omega_i^2} \tag{10}$$

3.2 Charge Regulated Surface Charge

Protein surface develops as a result of H^+ binding or dissociating at carboxylate and amine sites. Both can be written as acid dissociation processes with acid dissociation constant pK_s[26,27],

$$-\mathrm{COOH} \quad \rightleftharpoons \quad -\mathrm{COO}^- + \mathrm{H}^+ \ \ (\mathrm{p}K_{s=\mathrm{COOH}}) \tag{11}$$

$$-\mathrm{NH}^+ \quad \rightleftharpoons \quad -\mathrm{N} + \mathrm{H}^+ \ \ (\mathrm{p}K_{s=\mathrm{NH}}) \tag{12}$$

$$\tag{13}$$

The average total surface charge is the sum $\sigma = \sum_s \sigma_s$ over the charge for each site,

$$\sigma_s = q_s e N_s + e\Gamma_s^H. \tag{14}$$

q_s is the valency of the dissociated site, -1 for carboxylate and 0 for amine sites. N_s is the site density. Γ_s^H describes the degree of chemisorption of H^+ at each site

$$\Gamma_s^H = \frac{N_s a_H}{A_s K_s} \tag{15}$$

where $A_s = 1 + a_H/K_s$ is the inverse of the fraction of fully dissociated sites, In this model we assume that chemisorption involves only the H^+ ion, neglecting more subtle effects driven, for example, by competitive chemisorption of metal ions[28].

The quantity a_H here is defined strictly from the bulk hydrogen concentration c_{H0} (corresponding to pH 7.15) as[27]

$$a_H = c_{H0} \exp\left(\frac{-e\psi_0}{kT}\right) \tag{16}$$

where ψ_0 is the surface potential $\psi(x=0)$. It is important to note that a_H is *not* the activity of the hydrogen ion at the protein surface[27], which in the presence of the nonelectrostatic interaction $\mu_{H0}^{\rm NES}$ of the hydrogen ion (and neglecting activity coefficients which describe ion-ion interactions) would be $c_{H0}\exp[-(e\psi_0 + \mu_{H0}^{\rm NES})/kT]$. We refer to a_H as a "partial ion activity".

The number of each charge site for lysozyme is known[29,30], corresponding to the amino acid composition of the protein. We estimate surface site densities N_s as the number of sites spread homogeneously over the spherical protein surface. We apply the acid dissociation constants determined by Kuehner et al. from charge titrations[30], which enable a better match to experimental zeta potentials than the older set of constants presented by Tanford[29]. Surface charge parameters are collated in Table 3.

4 Results and Discussion

We determine the electrostatic potential outside the lysozyme surface by solving the Poisson-Boltzmann model, Eq. (1) and Eq. (2), including ion dispersion interactions, Eq. (4). We define the calculated zeta potential as the value of the electrostatic potential at a distance of 3 water molecules (3 diameters), that is at $z = 6.84$Å, taking the hard sphere radius of water[19] as 1.14Å. Calculated zeta potentials are shown in Fig. 1, compared against experimental values. With ion dispersion interactions included, theory reproduces experimental well, with values matching within ± 5 mV. Importantly the buffer-specific effect, the buffer Hofmeister series, is reproduced, showing buffers in the order Tris > cacodylate > phosphate > citrate. Significantly, theory is also able to reproduce charge reversal observed in citrate buffer, where a negative zeta potential was measured for lysozyme.

We emphasize that the agreement between theory and experiment seen in Fig. 1 has been achieved without the use of fitted parameters. Ion, buffer and protein properties have been determined either through the use of quantum chemical calculations (for ion polarizabilities, and size, determining dispersion coefficients) or by experimental measurement (charge regulation parameters for lysozyme). It is therefore worth considering how the zeta potential is predicted to change as buffer concentration varies. The calculated zeta potential is shown in Fig. 2 as a function of buffer concentration.

Interestingly, strong buffer-specific effect is found even at extremely low buffer concentrations, with $\Delta\zeta = 14$ mV between Tris and citrate at 1μM. We discuss this point further below.

We find that all anionic buffer solutions will achieve charge reversal at sufficiently high buffer concentration (obviously charge reversal is not induced by the cationic buffer Tris). The critical charge reversal buffer concentration is 6 mM, 25 mM and 40 mM for citrate, phosphate and cacodylate, respectively.

Maximum charge reversal is found at a buffer concentration 2 or 3 times greater than the critical charge reversal concentration,

Table 1 Properties of ions and neutral buffer molecules. a_i is Gaussian radius (Eq. (5)), permanent dipole moment μ, static polarizability α_0 in vacuum, dispersion coefficient B_i (Eq. (6)) interacting with protein surface, ion (molecule) valency, acid dissociation constant (pK) for buffer pairs

Species	a_i (Å)	μ (D)	α_0 (Å^3)	B_i (10^{-50} Jm^3)	valency	pK
Tris	2.70	2.06	10.99	-12.50	0	8.072
Tris$-$H$^+$	2.67	3.95	10.07	-11.49	+1	
Cacodylate	2.54	3.68	11.70	-12.79	-1	6.3
Cacodylic Acid	2.48	8.47	9.35	-10.61	0	
hydrogen phosphate	2.32	5.59	9.90	-10.42	-2	7.21
dihydrogen phosphate	2.26	5.43	6.77	-7.33	-1	
citrate	3.02	3.35	21.19	-23.47	-3	6.396
hydrogen citrate	2.98	2.73	17.30	-20.18	-2	
$[Na\cdot 3H_2O]^+$	2.25	0	4.14	-2.58	+1	
Cl^-	1.86	0	4.86	-4.87	-1	
nitrate	2.01	0.961	5.02	-5.56	-1	
SCN^-	2.18	1.43	8.13	-8.86	-1	
H_3O^+	0.974	1.64	0.963	-1.99	+1	
$[OH\cdot 3H_2O]^-$	2.39	0.566	7.31	-6.64	-1	

Table 2 Oscillator weights α_i (Å^3) and oscillator frequencies ω_i (eV) for five-mode decompositions of the dynamic electronic polarizabilities in vacuum of buffer and other ions (see Eq.10). α_0 is the static polarizability at $\omega = 0$

Ion	α_0 (Å^3)	mode 1		mode 2		mode 3		mode 4		mode 5	
		α_1	ω_1 (eV)	α_2	ω_2 (eV)	α_3	ω_3 (eV)	α_4	ω_4 (eV)	α_5	ω_5 (eV)
Tris	10.986	2.621	9.4880	6.708	17.7733	1.597	37.8701	0.0598	123.6151	–	–
Tris$-$H$^+$	10.067	3.288	11.7885	5.642	20.2507	1.098	42.9752	0.0386	144.1076	–	–
Cacodylate	11.704	1.980	4.6944	5.326	10.4813	3.941	20.1305	0.4202	52.7369	0.037	179.6642
Cacodylic Acid	9.347	1.516	7.4632	5.490	13.8460	2.083	25.8524	0.2361	67.6610	0.022	217.5881
hydrogen phosphate	9.903	1.510	3.1806	3.829	7.4202	3.789	17.9755	0.7249	43.7498	0.047	160.5765
dihydrogen phosphate	6.770	1.214	6.8266	3.153	13.3498	2.081	25.5990	0.2982	61.8246	0.024	211.2226
citrate	21.187	3.456	3.3290	7.160	8.2903	8.133	17.8210	2.3361	38.7816	0.100	124.5338
hydrogen citrate	17.297	2.565	5.7369	7.663	11.7658	5.975	23.3381	1.0478	50.4915	0.045	162.3418
$[Na\cdot 3H_2O]^+$	4.140	0.799	9.5637	2.140	17.1706	1.029	32.8362	0.164	73.0301	0.0076	253.7613
Cl^-	5.035	1.556	5.8045	2.593	11.0046	0.683	23.2807	0.0203	78.4509	0.0082	301.8525
nitrate	5.022	1.717	6.9016	1.940	15.3415	1.140	28.9292	0.215	65.9835	0.0092	253.7512
SCN^-	8.128	1.693	5.3557	4.510	10.1338	1.744	20.5960	0.164	53.2246	0.0164	254.5735
H_3O^+	0.9629	0.319	16.3084	0.553	26.7435	0.0873	59.3184	0.0035	211.7261	–	–
$[OH\cdot 3H_2O]^-$	7.305	1.218	5.6995	3.333	12.0142	2.385	24.0940	0.352	57.6833	0.0169	189.1787

Table 3 Lysozyme surface charge parameters. n, total number of sites per whole protein. N_s, site density assuming all charge sites are located on protein surface (spherical radius $R_p = 1.53$ nm). q_s, charge (in units of e) of dissociated site. pK_s, chemisorption dissociation constant for H$^+$ at the site. Parameters from Ref. 30 (tyrosine sites have been averaged to one group, following Kuehner's treatment of aspartate, lysine)

Site	n	N_s (sites/nm^2)	q_s	pK_s
aspartate	7	0.2380	-1	2.9
glutamate-7	1	0.0340	-1	2.6
glutamate-35	1	0.0340	-1	6.1
histidine	1	0.0340	0	5.8
lysine	6	0.2040	0	10.6
arginine	11	0.3739	0	12.77
tyrosine	3	0.1020	-1	10.73
terminal C (leucine)	1	0.0340	-1	3.1
terminal N (lysine)	1	0.0340	0	7.9

where the zeta potential achieves its largest (in magnitude) negative value. Above that concentration the negative charge reversed zeta potential weakens back towards zero, due to increased electrostatic screening.

4.1 Buffer Concentration and Ionic Strength

Up to this point we have compared buffer solutions at the same buffer concentrations, that is the same total buffer concentrations combining both the acidic and basic buffer species. Since the charges of acidic and basic species in general varies for each species, this means each buffer solution for the same buffer concentration has a different ionic strength. Some variation in protein properties such as zeta potential is therefore to be expected simply due to this variation in ionic strength. Nevertheless we emphasize that ionic strength alone cannot explain the observed buffer specific effect. In particular high ionic strength alone cannot explain the charge reversal from positive to negative zeta potential observed with citrate buffer and with added salt. High ionic strength alone would simply push the zeta potential towards zero, not cause it to cross over to negative values. This point is shown in Fig. 3a, showing the zeta potential as a function of ionic strength (including background H$^+$ and OH$^-$) with the ionic dispersion potential of Eq. (4) switched off ($\mu_i^{\mathrm{NES}} = 0$ in the Boltzmann relation, Eq. (2)). The zeta potential in NaCl without buffer is also also shown for comparison at the same ionic strength.

Significantly, similarly to Fig. 2, strong buffer specificity is still found at low ionic strength even without ionic dispersion interactions. Citrate continues to give a nearly 10 mV shift in zeta potential compared to other buffers at an ionic strength of 0.1 mM. The low concentration sensitivity can be understood through the nonlinear charge regulation relationship, Eq. (14), Eq. (15) and Eq. (16), between surface potential and protein charge[3]. Protein charge depends not only on bulk pH but also on surface poten-

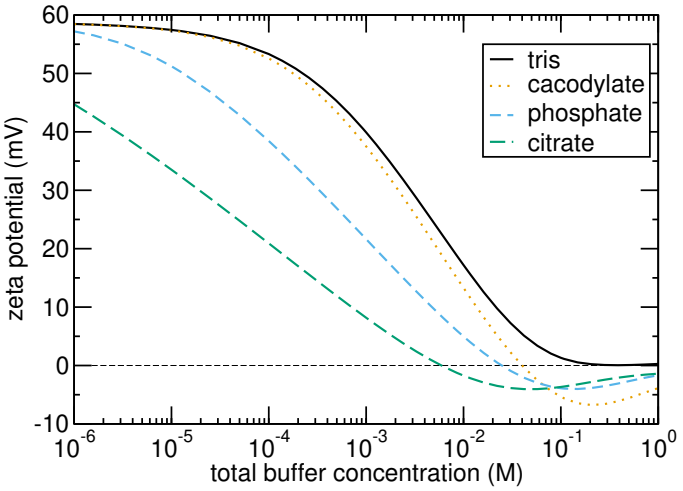

Fig. 2 Calculated zeta potentials for lysozyme in Tris, cacodylate, phosphate, citrate at pH 7.15, as a function of buffer concentration. Pure buffer solutions without added salt are shown here.

tial. At the same ionic strength the Debye length is the same in each buffer solution, but even long range decay is strictly speaking only characterized by the Debye length for simpler 1:1 electrolytes[31,32]. Close to the surface, valency-dependency in the surface potential can be expected. The capacitance (that is, the charge/potential relationship) of protein molecules is nontrivial.

The additional nonelectrostatic physisorption of anions driven by dispersion forces is required to explain charge reversal in the buffered lysozyme system considered here. In Fig. 3b we show calculated zeta potentials as a function of total ionic strength of pure buffer solutions (without added salt), now including ion dispersion interactions, Eq. (4). Pure NaCl solution (without buffer) is shown for comparison.

Valency-dependent buffer specificity is again observed at low ionic strengths, but buffer specificity becomes stronger, and the point of widest buffer specificity shifts to lower ionic strength, $\Delta\zeta = 24$ mV between Tris and citrate at an ionic strength of 0.2 mM, compared to $\Delta\zeta = 13$ mV at 1mM in the absence of ion dispersion interactions. All anionic buffer solutions eventually exhibit charge reversal due to adsorption of buffer anions induced by the dispersion interaction, consistent with the trend seen with increasing buffer concentration in Fig. 2. Naturally, charge reversal is not found with the cationic Tris buffer.

Interestingly, the high concentration turning point of strongest charge reversal becomes standardized at a common ionic strength around 200 mM. At this point the Debye length (0.7 nm at 200 mM) roughly matches the typical spatial range of ion dispersion interactions. Some buffer specificity is still found in the charge reversal concentration, with ionic strength 33 mM for citric, 48 mM for phosphate, but cacodylate reaches charge reversal at nearly the same ionic strength as citrate.

5 Discussion of dispersion interactions

In Fig. 4 we present the interaction potentials for the higher-valency member of each buffer ion pair. For the purpose of comparing the strength of the electrostatic and ion dispersion interaction energies, the absolute value of the interaction energy is shown, with the signed potentials presented in the insets. Dispersion interaction energies are attractive (negative) for all ions. Electrostatic ion interactions are attractive in the case of cacodylate and phosphate, repulsive in the case of Tris and citrate. The citrate electrostatic interaction is repulsive because of charge reversal, a consequence of the strong dispersion interaction of citrate at the protein interface. In fact for all buffer ions the dispersion interaction is more than 5 times stronger than the electrostatic interaction at the protein surface.

We consider the length scale of the ion dispersion interaction to be an important factor in buffer specificity. This can be characterized by the crossing point at which the electrostatic and ion dispersion energies become equal in magnitude. The crossing point for Tris$-H^+$ is similar to the radius of the ion, indicating that the electrostatic interaction dominates over dispersion once the Tris ion is no longer in contact with the surface. This case could be modelled using the idea of specific binding (chemisorption)[33]. But the crossing point of cacodylate and hydrogen phosphate lies outside the ion radius, indicating the role of the dispersion interaction as nonelectrostatic physisorption, active at a distance from the surface. The crossing point for citrate lies at 6.4 Å, well past the region of direct surface contact. That is, referring the zone of direct ion surface contact as the Helmholtz layer, we find that the dispersion interaction is significant (stronger than the electrostatic interaction) in the diffuse ion layer outside the Helmholtz layer.

It is significant that protein charge reversal is achieved through the dispersion interactions of negative buffer ions at low millimolar concentrations, even with monovalent buffer (cacodylate). Charge reversal may also occur as a consequence of ion-ion correlation[34,35], but correlation effects are associated with high ion concentrations, typically exceeding 1M for monovalent ions, 100 mM for divalent ions. In the case of trivalent citrate these two mechanisms for charge reversal, ion dispersion on the one hand and ion correlations on the other, may be in competition. But other buffers may still induce charge reversal through dispersion physisorption in conditions where correlation effects are not expected to be significant.

The buffer model presented here required a representation of cosmotropic small ions, Na^+ in particular, using explicit hydration. Explicit water in this case expresses short-range ion-water interactions in the context of the Mahanty-Ninham model of ion dispersion forces in which solvent medium penetrates the volume of the ion. This approach introduces a discrepancy by handling cosmotropic small ions with explicit water while other ions (including chaotropic Cl^-) are treated without explicit water. This discrepancy can be resolved in the context of a continuum model through the introduction of an ion cavity[18,36,37]. Application of a cavity model to protein interactions will require careful treatment of both the cavity energy and interface energy at the protein-solvent interface[38].

6 Conclusion

We have presented a theory that describes buffer specific effects observed in zeta potential measurements of lysozyme, including

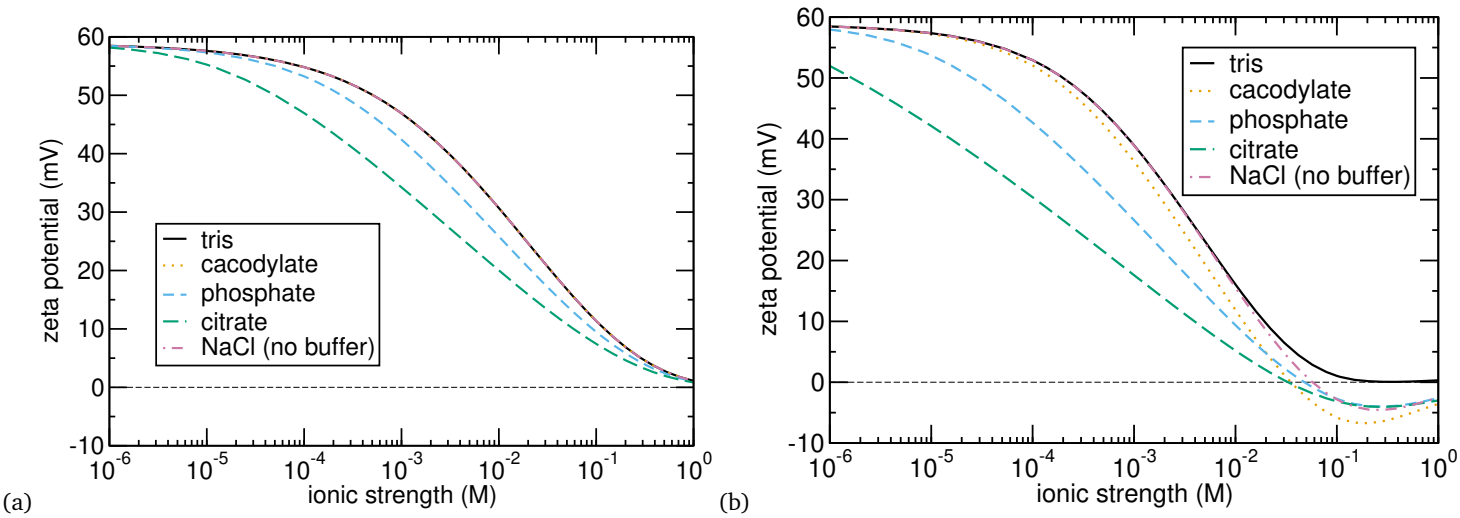

Fig. 3 Calculated zeta potentials for lysozyme. (a) Calculated with purely electrostatic theory neglecting all ion dispersion interactions. (b) Calculated including buffer ion dispersion interactions. Calculations made in Tris, cacodylate, phosphate, citrate at pH 7.15, as a function of total ionic strength. Pure buffer solutions without added salt are shown here. NaCl solution without buffer is also shown for comparison.

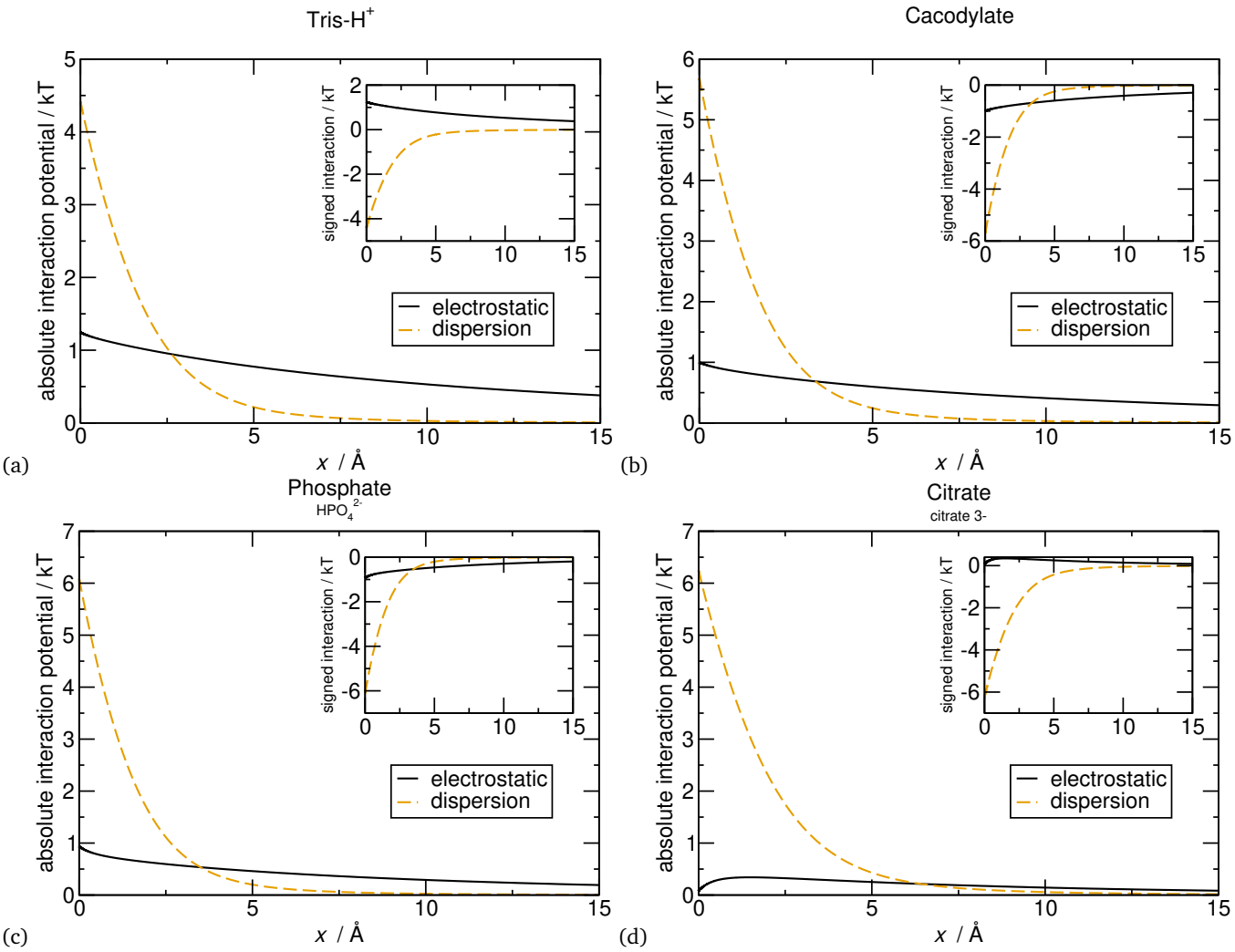

Fig. 4 Ion-lysozyme interaction potentials, comparing electrostatic and ion dispersion energies (kT units) for the higher-valency member of each buffer ion pair. (a) Tris-H^+, (b) cacodylate (1^-), (c) phosphate (HPO_4^{2-}), (d) citrate (3^-). Electrostatic interactions are evaluated for 10 mM buffer concentrations at pH 7.15.

charge reversal. Key elements of the theory are the incorporation of ion dispersion interactions (including buffer ions) into a Poisson-Boltzmann description of the electrolyte, together with a charge-regulated description of protein surface charge. The size and polarizability of cosmotropic small ions (Na^+, H^+, OH^-) are taken with explicit water, although this may be considered an implementation detail of the model of ion dispersion forces employed. Charge reversal (of lysozyme) is predicted with all anionic buffers at 10–50 mM buffer concentrations, with maximal charge reversal at total ionic strength around 200 mM. Valence-based buffer specificity is found at low buffer concentrations, with citrate continuining to give a 10 mV reduction in zeta potential even at 1 μM concentrations. Charge reversal driven by buffer ion dispersion forces is predicted even in low-valency buffers where ion correlation effects are not expected to be significant.

Author Contributions

DFP: Conceptualization, Formal analysis, Investigation, Methodology, Resources, Software, Writing – original draft. CC: Formal analysis, Investigation, Writing – review & editing. AS: Conceptualization, Funding acquisition, Investigation, Writing – review & editing.

Conflicts of interest

There are no conflicts to declare.

7 Acknowledgements

We acknowledge the grant of resources from the National Computational Infrastructure (NCI) , which is supported by the Australian Government. This was supported by resources provided by the Pawsey Supercomputing Centre with funding from the Australian Government and the Government of Western Australia. We also acknowledge computational support from CINECA, the national computational infrastructure of Italy. FIR2020, Fondazione di Sardegna (FdS, F72F20000230007), and Regione Autonoma della Sardegna (RASSR79857) are gratefully acknowledged. C.C. thanks MIUR (PON-AIM Azione I.2, DD 407-27.02.2018, AIM1890410-2) for funding.

Notes and references

1 P. Lo Nostro and B. W. Ninham, *Chemical Reviews*, 2012, **112**, 2286–2322.
2 B. Kang, H. Tang, Z. Zhao and S. Song, *ACS Omega*, 2020, **5**, 6229–6239.
3 D. F. Parsons and A. Salis, *Current Opinion in Colloid and Interface Science*, 2016, **23**, 41–49.
4 A. Salis, M. C. Pinna, D. Bilaničová, M. Monduzzi, P. Lo Nostro and B. W. Ninham, *Journal of Physical Chemistry B*, 2006, **110**, 2949–2956.
5 F. Cugia, M. Monduzzi, B. W. Ninham and A. Salis, *RSC Advances*, 2013, **3**, 5882–5888.
6 D. Roberts, R. Keeling, M. Tracka, C. F. van der Walle, S. Uddin, J. Warwicker and R. Curtis, *Molecular Pharmaceutics*, 2015, **12**, 179–193.
7 A. Salis and M. Monduzzi, *Current Opinion in Colloid & Interface Science*, 2016, **23**, 1–9.
8 F. Cugia, S. Sedda, F. Pitzalis, D. F. Parsons, M. Monduzzi and A. Salis, *RSC Advances*, 2016, **6**, 94617–94621.
9 C. A. Poole, H. C. Reilly and M. H. Flint, *In Vitro*, 1982, **18**, 755–765.
10 A. Salis, L. Cappai, C. Carucci, D. F. Parsons and M. Monduzzi, *The Journal of Physical Chemistry Letters*, 2020, **11**, 6805–6811.
11 A. Salis, D. Bilaničová, B. W. Ninham and M. Monduzzi, *The Journal of Physical Chemistry B*, 2007, **111**, 1149–1156.
12 L. Chen, K. O. Hodgson and S. Doniach, *Journal of Molecular Biology*, 1996, **261**, 658–671.
13 J. Mahanty, *Nuovo Cimento della Societa Italiana di Fisica, B: General Physics, Relativity, Astronomy, and Plasmas*, 1974, **22**, 110.
14 J. Mahanty and B. W. Ninham, *Dispersion Forces*, Academic Press, London, 1976.
15 M. Boström, E. R. A. Lima, E. C. Biscaia, F. W. Tavares, P. L. Nostro, D. F. Parsons, V. Deniz and B. W. Ninham, *The Journal of Physical Chemistry B*, 2009, **113**, 8124–8127.
16 J. Fiedler, M. Boström, C. Persson, I. Brevik, R. Corkery, S. Y. Buhmann and D. F. Parsons, *The Journal of Physical Chemistry B*, 2020, **124**, 3103–3113.
17 H. BOROUDJERDI, Y. KIM, A. NAJI, R. NETZ, X. SCHLAGBERGER and A. SERR, *Physics Reports*, 2005, **416**, 129–199.
18 J. Fiedler, P. Thiyam, A. Kurumbail, F. A. Burger, M. Walter, C. Persson, I. Brevik, D. F. Parsons, M. Boström and S. Y. Buhmann, *Journal of Physical Chemistry A*, 2017, **121**, 9742–9751.
19 D. F. Parsons and B. W. Ninham, *Journal of Physical Chemistry A*, 2009, **113**, 1141–1150.
20 F. W. Tavares, D. Bratko, H. W. Blanch and J. M. Prausnitz, *J. Phys. Chem. B*, 2004, **108**, 9228–9235.
21 D. F. Parsons and B. W. Ninham, *Langmuir*, 2010, **26**, 1816–1823.
22 R. Ahlrichs, M. Bär, M. Häser, H. Horn and C. Kölmel, *Chemical Physics Letters*, 1989, **162**, 165–169.
23 C. Adamo and V. Barone, *Journal of Chemical Physics*, 1999, **110**, 6158–6170.
24 A. K. Wilson, D. E. Woon, K. A. Peterson and J. Thom H. Dunning, *Journal of Chemical Physics*, 1999, **110**, 7667–7676.
25 K. A. Peterson and J. Thom H. Dunning, *Journal of Chemical Physics*, 2002, **117**, 10548–10560.
26 D. F. Parsons and A. Salis, *The Journal of Chemical Physics*, 2015, **142**, 134707.
27 D. F. Parsons and A. Salis, *Journal of Chemical Physics*, 2019, **151**, 024701.
28 D. F. Parsons, T. T. Duignan and A. Salis, *Interface Focus*, 2017, **7**, 20160137.
29 C. Tanford and R. Roxby, *Biochemistry*, 1972, **11**, 2192–2198.
30 D. E. Kuehner, J. Engmann, F. Fergg, M. Wernick, H. W. Blanch and J. M. Prausnitz, *The Journal of Physical Chemistry B*, 1999, **103**, 1368–1374.

31 M. A. Knackstedt and B. W. Ninham, *The Journal of Physical Chemistry*, 1996, **100**, 1330–1335.
32 M. M. Kohonen, M. E. Karaman and R. M. Pashley, *Langmuir*, 2000, **16**, 5749–5753.
33 J. H. Jordan, H. S. Ashbaugh, J. T. Mague and B. C. Gibb, *Journal of the American Chemical Society*, 2021, **143**, 18605–18616.
34 A. Y. Grosberg, T. T. Nguyen and B. I. Shklovskii, *Reviews of Modern Physics*, 2002, **74**, 329–345.
35 R. Kjellander, *Journal of Physics: Condensed Matter*, 2009, **21**, 424101.
36 T. T. Duignan, D. F. Parsons and B. W. Ninham, *Journal of Physical Chemistry B*, 2013, **117**, 9421–9429.
37 T. T. Duignan, D. F. Parsons and B. W. Ninham, *Journal of Physical Chemistry B*, 2014, **118**, 3122–3132.
38 T. T. Duignan, D. F. Parsons and B. W. Ninham, *Chemical Physics Letters*, 2015, **635**, 1–12.